MODELING AND ADAPTIVE NUMERICAL TECHNIQUES FOR OXIDATION OF CERAMIC COMPOSITES

S. Adjerid, M. Aiffa, J. E. Flaherty, J. B. Hudson, M. S. Shephard

Scientific Computation Research Center
Rensselaer Polytechnic Institute
Troy, NY 12180-3590

ABSTRACT

We develop a mathematical model for the oxidation of silicon carbide in a crack or pore. The model consists of a nonlinear partial differential system that is solved by adaptive finite element software that automates many of the computational decisions.

1. INTRODUCTION

Oxidation shortens the life of ceramic matrix composites by, e.g., changing the elastic properties of the medium, reducing bonding strength due to a loss of fiber coatings, and weakening fibers through reaction [1-3]. Composite materials are protected by coatings; however, cracks that form as a result of thermal or other loading may expose the matrix and fibers to hostile environments. We present a model for the oxidation of a cracked silicon carbide (SiC) matrix that is exposed to a hot gaseous mixture of oxygen and water. The gases diffuse into the matrix and react with the SiC to form a layer of silicon dioxide (SiO_2) between the gaseous mixture and the SiC. The oxidation proceeds into the composite at a rate that is controlled by the solid-state diffusion of oxygen and/or water vapor in SiO_2. Phase transformations due to the oxidizing reactions are accompanied by a volume expansion that causes the viscous SiO_2 to flow and fill the crack [1-3]. This may reduce damage to the composite. The model, consisting of a nonlinear partial differential system, is solved by adaptive finite element software [4] with capabilities for unstructured mesh generation and combinations of automatic mesh refinement/coarsening (h-refinement), method-order variation (p-refinement), and mesh motion (r-refinement). Adaptivity helps control numerical accuracy and track moving material boundaries; hence, it provides an effective tool for solving oxidation and related [5] composite fabrication problems. The model and its solution by the adaptive software produce an efficient way to predict and understand changes in the chemical, physical, and mechanical properties of composites that will eventually lead to improved design and longer material life.

2. OXIDATION MODEL

Following [2,3], we expose a SiC matrix to O_2 and H_2O that are absorbed into the matrix and react with SiC according to the overall reaction

$$3SiC_{(s)} + 5O_{2_{(g)}} \rightarrow 3SiO_{2_{(s)}} + CO_{2_{(g)}} + 2CO_{(g)}, \tag{1a}$$

$$SiC_{(s)} + 3H_2O_{(g)} \rightarrow SiO_{2_{(s)}} + CO_{(g)} + 3H_{2_{(g)}}. \tag{1b}$$

These reactions occur at the interface between SiC and SiO_2 with O_2 and H_2O diffusing through SiO_2 to reach the fronts.

The solid matrix consists of a mixture of reactants and products. Let the mass $m_i\ (g)$ of chemical species i at time t in a control volume V be

$$m_i(t) = \int_V \rho Y_i \, d\omega, \quad i = 1, 2, \cdots, 7, \tag{2}$$

where ρ is the density of the mixture, Y_i is the mass fraction of species i and $d\omega$ is a volume element. Indices of the seven species involved in the reactions are listed in Table I. Considerations of mass conservation of species i yield

$$\frac{dm_i}{dt} = -\int_S \mathbf{J}_i \cdot \mathbf{n} \, d\sigma - \int_S \rho Y_i \mathbf{v} \cdot n \, d\sigma + \int_V \dot{q}_i \, d\omega, \quad i = 1, 2, \cdots, 7, \tag{3a}$$

where S is the boundary of V, $\mathbf{n}$ is a unit outer normal to S, $d\sigma$ is a surface element, $\mathbf{v}$ is the mixture velocity, and $\dot{q}_i$ and $\mathbf{J}_i$ are, respectively, the mass production rate and diffusive flux of species i. Assuming Fickian diffusion and regarding the position of a material point $\mathbf{x}$ as a function of t and its initial spatial location $\mathbf{X}$, we have

$$\mathbf{v}(\mathbf{X},t) = \frac{\partial \mathbf{x}(\mathbf{X},t)}{\partial t}, \quad \mathbf{J}_i = -D_i \nabla(\rho Y_i) \tag{3b,c}$$

with D_i being the diffusivity of species i in the mixture and ∇ being the gradient operator.

Applying the divergence theorem to (3a) while using (2) and (3c) yields

$$\frac{d(\rho Y_i)}{dt} = \nabla \cdot D_i \nabla(\rho Y_i) - \rho Y_i \nabla \cdot \mathbf{v} + \dot{q}_i, \quad \mathbf{x} \in \Omega(t), \quad t > 0, \tag{4a}$$

where

$$\frac{d(\rho Y_i)}{dt} = \frac{\partial(\rho Y_i)}{\partial t} + \mathbf{v} \cdot \nabla(\rho Y_i), \quad i = 1, 2, \cdots, 7, \tag{4b}$$

is the material derivative and $\Omega(t)$ is the spatial region occupied by the medium at time t.

Since mass production rates during high-temperature oxidation are much faster than diffusive rates, we assume all reactions are irreversible, isothermal, and have rates that are linear in each concentration to obtain

$$\dot{q}_1 = -5w_1M_1, \quad \dot{q}_2 = (2w_1+w_2)M_2, \quad \dot{q}_3 = w_1M_3, \quad \dot{q}_4 = -(3w_1+w_2)M_4,$$

$$\dot{q}_5 = (3w_1+w_2)M_5, \quad \dot{q}_6 = -3w_2M_6, \quad \dot{q}_7 = 3w_2M_7. \tag{5a-g}$$

where

$$w_1 = k_1\left[\frac{\rho Y_1}{M_1}\right]\left[\frac{\rho Y_4}{M_4}\right], \quad w_2 = k_2\left[\frac{\rho Y_4}{M_4}\right]\left[\frac{\rho Y_6}{M_6}\right]. \tag{5h,i}$$

The parameters k_1 and k_2 are the rate constants for rate-controlling steps in reactions (1a,b) and M_i denotes the molecular weight of species $i = 1, 2, \cdots, 7$ (cf. Table I). Thus, $\rho Y_i/M_i$, is the concentration of species i in mol/cm^3.

Table I. Index and molecular weight M_i (g) of species i.

Species	O_2	CO	CO_2	SiC	SiO_2	H_2O	H_2
i	1	2	3	4	5	6	7
M_i	32	28	44	40	60	18	2

Assuming that a control volume V contains only chemical constituents without voids between the compounds, Adjerid et al. [5] show that

$$\nabla\cdot\mathbf{v} = \sum_{i=1}^{7}\frac{1}{\hat{\rho}_i}[\dot{q}_i + \nabla\cdot D_i\nabla\rho Y_i], \quad \mathbf{x}\in\Omega, \quad t > 0. \tag{6}$$

where $\hat{\rho}_i$ is the theoretical density of species i. In typical situations, there is very little free O_2, H_2, H_2O, CO, and CO_2 in the matrix; therefore, it is reasonable to neglect the ρY_i terms on the right of (6) for $i = 1, 2, 3, 6, 7$. Additionally, D_4 and D_5 are negligible so (6) becomes

$$\nabla\cdot\mathbf{v} = \sum_{i=4}^{5}\frac{\dot{q}_i}{\hat{\rho}_i}. \tag{7}$$

The oxidizing reactions (1) are accompanied by nearly a 120% volume expansion that induces forces on the matrix causing it to flow. We assume that the material is capable of viscous deformation and describe its motion by the Navier-Stokes equations

$$\rho\frac{d\mathbf{v}}{dt} + \mathbf{v}[\frac{\partial\rho}{\partial t} + \nabla\cdot(\rho\mathbf{v})] = \nabla\cdot\mathbf{T} \tag{8a}$$

where the traction matrix $\mathbf{T}$ has components

$$T_{kl} = (-p + \lambda\nabla\cdot\mathbf{v})\delta_{kl} + \mu(\frac{\partial v_k}{\partial x_l} + \frac{\partial v_l}{\partial x_k}), \quad k, l = 1, 2, 3, \tag{8b}$$

with λ and μ being Lamé parameters, p being the pressure, and δ_{kl} being the Kronecker delta.

Initially, the matrix only contains SiC; thus, the initial conditions are

$$Y_i(\mathbf{X},0) = \begin{cases} 0, & i \neq 4 \\ 1, & i = 4, \end{cases} \quad i = 1, 2, \cdots, 7, \quad \mathbf{v}(\mathbf{X},0) = 0, \quad p(\mathbf{X},0) = 0. \tag{9}$$

Boundary conditions prescribe the crack surface as traction free

$$\mathbf{T}\cdot\mathbf{n} = 0, \quad \mathbf{x}\in\Gamma, \quad t > 0. \tag{10a}$$

On planes of symmetry and in the far field, we prescribe

$$\mathbf{v}\cdot\mathbf{n} = 0, \quad \mathbf{n}\cdot\nabla[\mathbf{v} - (\mathbf{v}\cdot\mathbf{n})\mathbf{n}] = 0, \quad D_i\nabla(\rho Y_i)\cdot\mathbf{n} = 0, \quad i = 1, 2, \cdots, 7. \tag{10b-d}$$

The rate of absorption and desorption of gaseous species i is assumed proportional to the deviation of Y_i from its maximum solubility s_i in SiO_2, $i = 1, 2, 3, 6, 7$; thus,

$$D_i\nabla(\rho Y_i)\cdot\mathbf{n} = -\phi_i(\mathbf{x}, Y_i - s_i), \quad i = 1, 2, 3, 6, 7, \quad \mathbf{x}\in\Gamma, \quad t > 0, \tag{10e}$$

where Γ is the surface of the crack and $\phi_i(\mathbf{x},z)$ is a saturation function as described in Section 3.

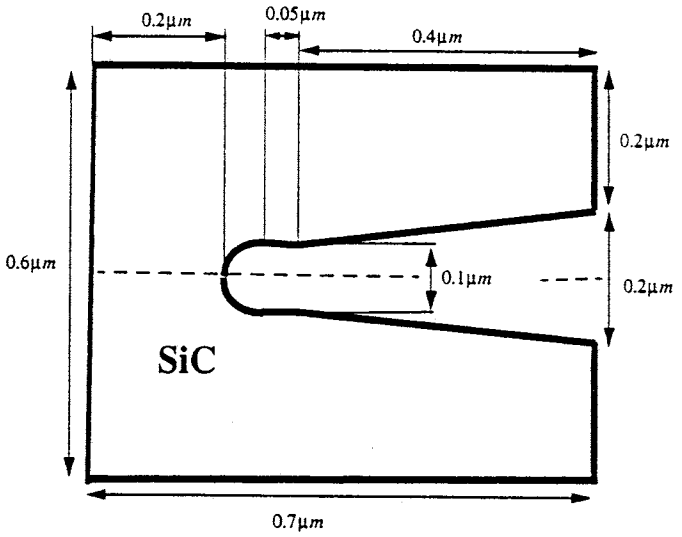

Figure 1. A two-dimensional *SiC* matrix containing a crack.

3. APPLICATION

We consider an idealized crack in a two-dimensional *SiC* matrix (cf. Figure 1) that is exposed to oxygen; thus, reaction (1b) is not present and H_2O and H_2 are not involved. With the geometry of Figure 1 and the specified reactants, we prescribe

$$\phi_i(\mathbf{x},z) = \begin{cases} -0.075zh(x_1)[1 + \tanh(10(x_1 - 2.5))], & i = 1, \\ 0, & i = 6 \\ 0.5\times 10^{-4}z\,[1 + \tanh(z\times 10^5)], & i = 2, 3, 7 \end{cases}, \tag{10f}$$

where $z = Y_i - s_i$ and $h(x_1)$ is half of the thickness of the crack at horizontal coordinate x_1. The topmost equation simulates a decrease in flux as the crack width narrows; the middle equation signifies that water vapor is not present in this example; and the bottom equation is a sharp but continuous transition from no flux to a saturation value.

A dimensionless version of the partial differential system (4, 5, 7-10) is solved using adaptive finite element software that has capabilities for automatic h-, p-, and/or r-refinement [4,5]. Although p-refinement is very efficient [4], we use hr-refinement with piecewise linear polynomials ($p = 1$). The r-refinement is used to follow evolving reaction zones and track the solid-gas interface as the matrix expands. The h-refinement is used to increase solution resolution near sharp transitions. Adaptive h-refinement is guided by two elemental error indicators: η_Δ is a mean-square average of jumps in $\partial \rho Y_4/\partial \mathbf{n}$ across the edges of element Δ and ζ_Δ is a similar average of jumps in the components of $\partial \mathbf{v}/\partial \mathbf{n}$ [6]. Letting $\bar{\eta}$ and $\bar{\zeta}$, respectively, denote averages of η_Δ and ζ_Δ over all elements, we refine those elements where $\eta_\Delta > 1.8\bar{\eta}$ or $\zeta_\Delta > 2.2\bar{\zeta}$. A vertex is scheduled for coarsening when the error indicators on all elements containing it are less than $0.3\bar{\eta}$ and $0.7\bar{\zeta}$. When this occurs, the low-error vertex is moved (''collapsed'') to its neighboring vertex having the largest interior angle. This eliminates elements and coarsens the mesh. Badly shaped elements that may result from r-refinement are eliminated by a combination of edge swapping (exchanging the diagonal of the quadrilateral formed by two triangular elements) and vertex collapsing [6]. The variable-step, variable-order time integration [4-6] was performed with a temporal error tolerance of 10^{-4} and was halted every five time steps to examine the error indicators and refine, coarsen, or move the mesh as necessary.

In order to overcome spurious pressure oscillations that arise in an (essentially) incompressible medium, we introduce an ''artificial compression'' and solve

$$\varepsilon \frac{dp}{dt} + \nabla \cdot \mathbf{v} = \sum_{i=4}^{5} \frac{\dot{q}_i}{\hat{\rho}_i} \tag{11a}$$

instead of (7b). This stabilizes the viscous flow while not greatly affecting accuracy when ε is small. We choose

$$\varepsilon = \frac{\bar{\varepsilon} L^2}{\mu_5 D_1 s_1} \tag{11b}$$

where L $(= 0.7\ \mu m)$ is the length of Ω (cf. Figure 1), μ_5 is the viscosity of SiO_2, and $\bar{\varepsilon}$ was selected as 10^{-6}.

Dimensionless variables are obtained by scaling $\mathbf{x}$ by L, ρ by $\hat{\rho}_5$, t by $D_1 s_1/L^2$, and p by $\mu_5 L^2/(\bar{\varepsilon} D_1 s_1)$. Using symmetry, we solve a problem on the upper half of the matrix shown in Figure 1. Those parameter values available in the literature [7] at an operating temperature of $1100°C$ are $D_1 = 6.6 \times 10^{-13}$, $D_6 = 3.6 \times 10^{-11}$ (m^2/s), $\hat{\rho}_4 = 3.2$, $\hat{\rho}_5 = 2.2$ (g/cm^3), and $\lambda_5 = \mu_5 = 10^{12}$ (Ns/m^2). The remaining parameters were estimated relative to these. For example, we selected $\lambda_4 = \mu_4 = 10^{15}\ Ns/m^2$ and assumed that the Lamé parameters for the mixture varied linearly between their SiC and SiO_2 values in the reaction zone; thus,

$$\lambda = \mu = \mu_5 + (\mu_4 - \mu_5) Y_4. \tag{12}$$

The higher values of the Lamé parameters for SiC simulate its greater stiffness (at $1100°C$) relative to SiO_2. The value of the reaction rate k_1 was selected as $2 \times 10^{-4} m^3/s$ to ensure diffusion dominance. Increasing or decreasing this value yielded similar results with sharper or more diffuse reaction zones, respectively. We assumed that the diffusivity of CO and CO_2 in SiO_2 is faster than that of O_2 and selected $D_2 = D_3 = 10^{-10} m^2/s$. Finally, maximum solubility limits were chosen as $s_i = 10^{-3}$, $i = 1, 2, 3$. Those parameters that remain unspecified are irrelevant to this

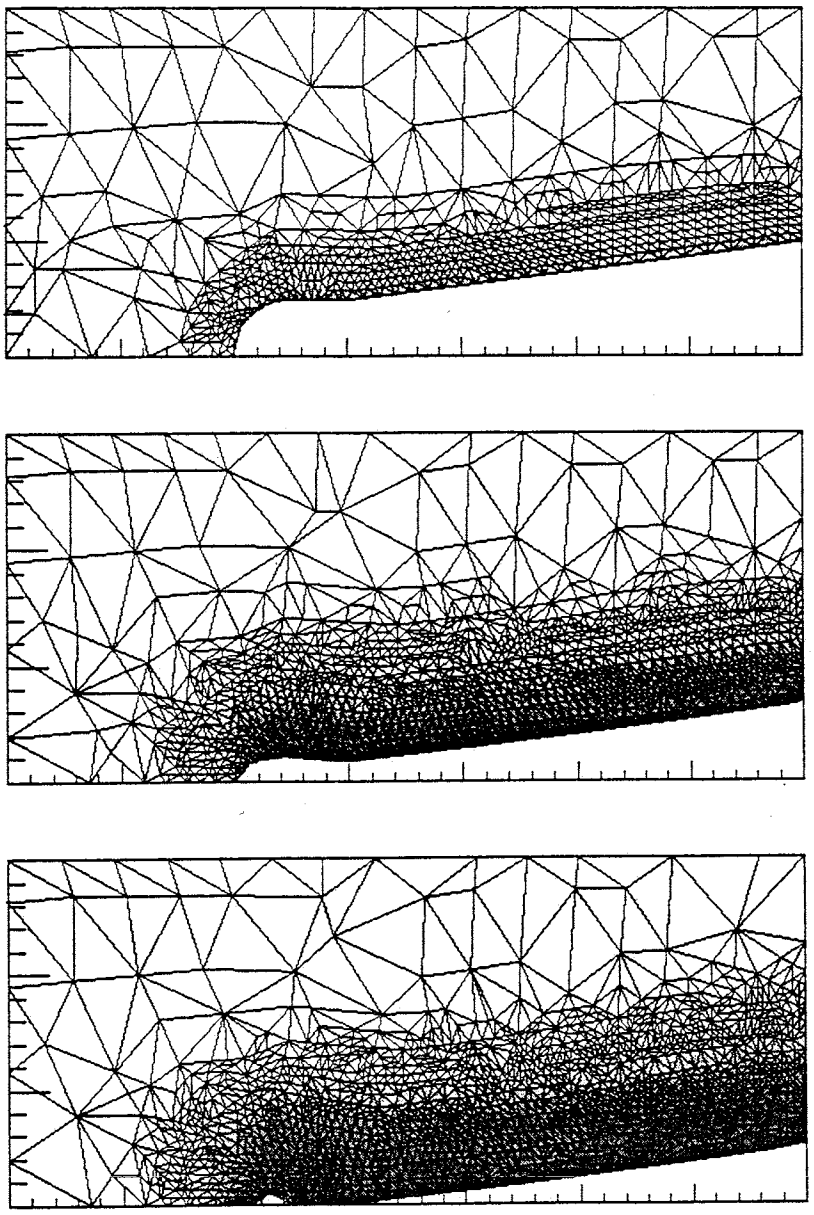

Figure 2. Mass fraction of *SiC* at $t = 0.2$, 1.77, and 3.6 min. Lighter shades indicate a high concentration of *SiC* and darker ones indicate a low concentration.

application.

The concentration of *SiC* and the corresponding adaptive meshes at $t = 0.2$, 1.77, 3.6 min are shown in Figure 2. In Figure 3, we show the pressure with velocity vectors superimposed at $t = 3.6$ min. The relative mass and volume changes $m(t)/m(0) - 1$ and $\Omega(t)/\Omega(0) - 1$ appear as functions of t in Figure 4. The oxidation

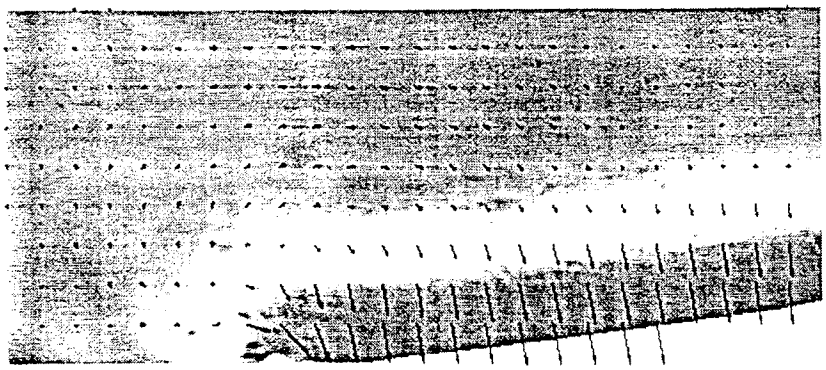

Figure 3. Pressure and velocity vectors at t = 3.6 min with lighter shading indicating higher pressures.

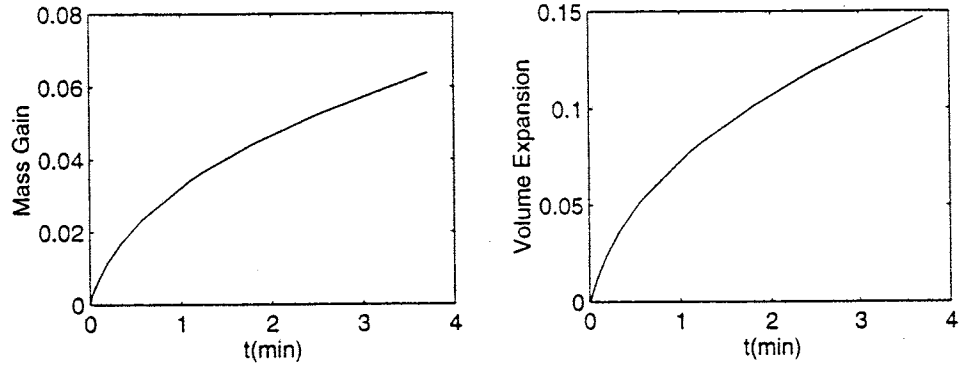

Figure 4. Total relative mass (left) and volume (right) changes vs. time.

front advances into the SiC matrix and SiO_2 flows into the crack to ultimately close it; thereby, reducing the gaseous diffusion into the matrix (cf. Figure 2). Figure 3 displays a qualitatively correct high pressure in the reaction zone and a flow of SiO_2 into the crack. The meshes of Figure 2 indicate that the adaptive software is placing fine meshes in the reaction zone where variables are changing rapidly while using coarse meshes elsewhere. The results of Figure 4 agree with experimental results [1,2] which predict that the system is diffusion-controlled; thus, indicating parabolic mass and volume change rates. Densities approach their correct theoretical values once reactions have passed.

4. DISCUSSION

We have developed a reaction-diffusion model to analyze the oxidation of ceramic composites. When used with adaptive finite element software, the model predicted qualitatively correct chemical and mechanical behavior and quantitatively correct mass gain. Our model displays a closing crack, which should inhibit

oxidation. We will integrate this software into an overall mechanism-based design system [8] that will simplify future analyses. Computational results will be compared with existing [1,2] and planned experiments.

Several improvements are possible. We are testing a model for the gaseous flow in the crack that contains a combination of Fickian and Knudsen diffusion. We will also include oxidation by H_2O as described herein. Coated and uncoated fibers will be added to the matrix with their associated reaction and surface diffusion models. Parameter studies will endeavor to determine how damage varies with crack geometry and operating conditions. Solving contact problems as the crack closes is an essential capability that must be developed. With this, elastic, visco-elastic, and/or visco-plastic deformations should be investigated and possibly included in the mechanical model. With these, it should be possible to predict the formation of cracks in the SiO_2 as oxidation progresses and stress patterns change. Coupling these micro-scale models with macro-mechanical models that anticipate the behavior of the composite structure are also envisioned [8].

ACKNOWLEDGEMENT

The authors gratefully acknowledge support of this project from ARPA/ONR under Grant N00014-92J-1779, "Mechanism-Based Design of Composite Structures," Steven Fishman and William Coblenz, Project Monitors.

References

1. L. Filipuzzi, G. Camus, R. Naslain, and J. Thebault, Oxidation Mechanisms and Kinetics of 1D-SiC/C/SiC Composite Materials: I, An Experimental Approach, *J. Am. Ceram. Soc.*, **77** (2), 459-466, 1994.

2. F. Lamouroux and G. Camus, Kinetics and Mechanisms of Oxidation of 2D Woven C/SiC Composites: I, Experimental Approach, *J. Am. Ceram. Soc.*, **77** (8), 2049-2057, 1994.

3. Y.G. Gogotsi and M. Yoshimura, Low-Temperature Oxidation, Hydrothermal Corrosion, and Their Effects on Properties of SiC (Tyranno) Fibers, *J. Am. Ceram. Soc.*, **78** (6), 1439-1450, 1995.

4. S. Adjerid, J.E. Flaherty, P.K. Moore, and Y.J. Wang, High-Order Methods for Parabolic Systems, *Physica D*, **60**, 94-111, 1992.

5. S. Adjerid, J.E. Flaherty, W. Hillig, J.B. Hudson, and M.S. Shephard, Modeling and the Adaptive Solution of Reactive Vapor Infiltration Problems, *Model. Simul. Mater. Sci. Engng.*, **3**, 737-752, 1995.

6. M. Aiffa, *Adaptive hp-Refinement Methods for Singularly Perturbed Elliptic and Parabolic Systems*, Ph.D. Dissertation, Dept. Math. Sci., Rensselaer Polytechnic Institute, Troy, 1997, in preparation.

7. R.H. Doremus, *Glass Science*, 2nd Ed., John Wiley & Sons, New York, 1994.

8. R. Wentorf, M.S. Shephard, G.J. Dvorak, J. Fish, M.W. Beall, R. Collar, and K.L. Shek, Software Frame for Mechanism-Based Design of Composite Structures, these proceedings, 1997.